JOURNAL OF RAMAN SPECTROSCOPY
J. Raman Spectrosc. **31**, 125–135 (2000)

Simulations of two-dimensional femtosecond infrared photon echoes of glycine dipeptide

Andrei Piryatinski, Sergei Tretiak, Vladimir Chernyak and Shaul Mukamel*
Department of Chemistry, University of Rochester, Rochester, New York 14627, USA

The multidimensional optical response of the amide I band of glycine dipeptide is calculated using a vibrational–exciton model, treating each peptide bond as a localized anharmonic vibration. The 2D photon echo signal is obtained by solving the non-linear exciton equations. Comparison of different models of spectral broadening (homogeneous and diagonal and off-diagonal static disorder) shows completely different 2D signals even when the 1D infrared spectra are very similar. The phase of the 2D signal may be used to distinguish between overtone and collective types of two-exciton states. Vanishing of the 2D signal along certain directions can be attributed to the variation of the phase. **Copyright © 2000 John Wiley & Sons, Ltd.**

INTRODUCTION

Vibrational spectra of the 1600–1700 cm^{-1} amide I band in proteins and polypeptides originate from the stretching motion of the CO bond coupled to in-phase N–H bending and C–H stretching. This mode has a strong transition dipole moment and is clearly distinguishable from other vibrational modes of the amino acid side-chains. Early study of symmetric model polypeptides conducted by Krimm and Bandeker[1] have demonstrated that the transition dipole–dipole interaction between the CO stretching modes results in the delocalization of amide I states, which can be thought of as Frenkel excitons of vibrational nature. The dependence of the coupling energy on relative orientations and distances of the interacting dipoles results in a unique amide I band signature of the particular secondary structure motif. This property is widely utilized in polypeptide and protein structure determination.[2–7] Good agreement with experiment has been obtained by Torii and Tasumi[8] in the model calculation of the absorption lineshape for a few mid-size (~100 peptide) globular proteins with known structures, assuming dipole–dipole coupling between peptide groups.

The information extracted from ordinary (one-dimensional, 1D) infrared spectra is limited since a protein usually folds into a complex three-dimensional structure, which consists of several polypeptide segments forming different types of secondary structures. The amide I band thus contains a number of unresolved spectral lines associated with vibrational motions of different structural elements of the protein. Conformational fluctuations within a particular three-dimensional protein structure and local interaction with solvent induce inhomogeneous broadening and the spectrum is highly congested. Fourier transform infrared (FTIR) spectroscopy has been employed to improve the resolution of these spectra.[2]

Multidimensional spectroscopic techniques[9–11] constitute an effective tool for probing complex proteins and polypeptide vibrational dynamics and could provide direct information on the nature of intramolecular and protein–solvent interactions. Non-linear femtosecond spectroscopy provides a multidimensional view of complex molecules and liquids and has the capability to disentangle ordinary poorly resolved linear (1D) spectra. The elimination of inhomogeneous broadening and cross peaks among multiple excitations provide most valuable dynamic and structural information.[12–14] Electronically resonant multidimensional techniques may be used to probe chromophore aggregate.[13,15,16] Nuclear (vibrational) and solvent dynamics have been probed using Raman and infrared spectroscopy.[17–21]

We should distinguish between off-resonant 2D Raman[9–11] and resonant IR[21–23] spectroscopy, which provide complimentary information on the vibrational dynamics. In the impulsive 2D Raman spectroscopy a sample is excited by a train of two pairs of optical pulses which prepare a superposition of quantum states. This superposition is probed by the scattering of the probe pulse. The electronically off-resonant pulses interact effectively with the electronic polarizability, which depends parametrically on the vibrational coordinates, corresponding to the fifth-order non-linear response. In 2D resonant IR spectroscopy the incoming pulses are directly coupled to the vibrational dipoles, inducing the third-order non-linear response.

A complete description of one- and two-exciton dynamics contributing to the 2D non-linear response is possible using the non-linear exciton equations (NEE).[24] The signal is represented in terms of one-exciton Green functions and two-exciton scattering matrix. Four coherent ultrafast 2D techniques based on the NEE solution have been proposed[25] and computer simulations of the 2D response were performed for model three-chromophore aggregates where each chromophore was modeled as a two-level system. It has been demonstrated that positions and absolute

* Correspondence to: Shaul Mukamel, Department of Chemistry, University of Rochester, Rochester, New York 14627, USA.
Contract/grant sponsor: National Science Foundation.
Contract/grant sponsor: United States Air Force Office of Scientific Research.

CCC 0377–0486/2000/020125–11 $17.50
Copyright © 2000 John Wiley & Sons, Ltd.
Received 17 July 1999
Accepted 28 July 1999

values of cross peaks provide information on the chromophore coupling strength and consequently on aggregate geometry.

Experimental 2D IR studies of carbonyls were carried out by Rector *et al.*[21] and 2D studies of the amide I spectral region of small proteins such as apamin, scyllatoxin and bovine pancreatic trypsin inhibitor (BPTI) were reported by Hamm *et al.*,[22] who employed 2D IR incoherent femtosecond pump–probe and dynamic hole burning experiments. In this study the anharmonicity, relaxation and energy equilibration times were measured, and the disorder-induced delocalization length of vibrational excitons was estimated. Similarly to 2D NMR spectroscopy,[26,27] the sensitivity of 2D IR signal to protein geometry can be used for structure determination. This has been demonstrated experimentally on a model pentapeptide cyclo-Abu-Arg-Gly-Asp-Mamb molecule,[23] the structure of which is known from x-ray and NMR studies.[28] The cross-peak positions and intensities were detected by dynamic hole burning measurements and the coupling energies between the amide groups were determined.

In this work, we applied the NEE to compute 2D vibrational IR photon echoes (PE)[25] from glycine dipeptide ($CH_3CONHCH_2CONHCH_3$). This molecule has two CO bonds, each modeled as a three vibrational level system. Our calculations set the stage for the analysis of 2D spectra of longer polypeptides and proteins. In the next section we calculate one- and two-vibrational–exciton states of glycine dipeptide including diagonal and off-diagonal static disorder. In the subsequent section we present numerical simulations of 2D PE signal for different (homogeneous and inhomogeneous) models of spectral broadening. We then examine the phase of the signal and show that it has a distinct values characteristic for the resonances associated with various types of two-exciton states. Interference in certain directions is an important signature of 2D signals.

VIBRATIONAL–EXCITON MODEL OF GLYCINE DIPEPTIDE

Geometry optimization and normal modes of the glycine dipeptide were computed at the density functional B3LYP6–31+G(d) level using Gaussian 98.[29] The optimized structure is shown in Fig. 1. The molecule has two identical peptide units, N5C2O3 and N9C7O8, which form the amide I vibrational band. The CO bond length is 1.23 Å and the NC bond (within a peptide unit) length is 1.36 Å. Each CO bond has a dipole placed 0.868 Å from the carbon atoms. The distance between the dipoles is $|\mathbf{R}_{12}| = 4.44$ Å. Their orientations are set 25° with respect to CO bonds. The angle between the dipole moments is 117°. The angle between the first dipole (N5C2O3 group) and the vector $\mathbf{R}_{12}$ is 156° and that of the second dipole is 87°. These parameters are consistent with previous studies of polypeptides.[1,8,22,23] The vibrational normal modes have been reported.[30,31]

The vibrational dynamics, including coupling to the radiation field, is described by the interacting exciton Hamiltonian given by Eqn (2.4) in Ref. 25. We shall keep the notations of this paper. The localized high-wavenumber anharmonic CO stretching modes are modeled as primary excitations. Dipole–dipole interaction

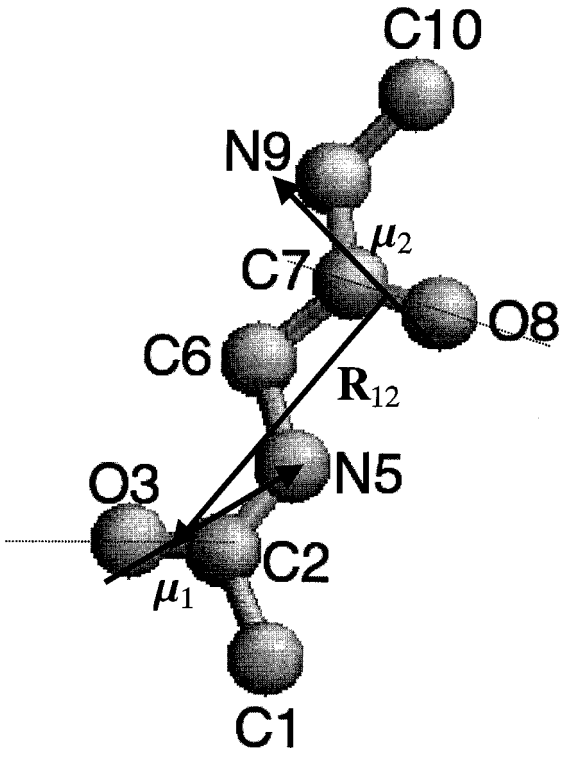

Figure 1. Optimized geometry of glycine dipeptide. Transition dipole moments of each peptide unit is denoted μ_1 and μ_2. $\mathbf{R}_{12}$ is the vector connecting their positions.

between CO vibrations leads to the formation of delocalized vibrational Frenkel excitons:

$$|e_1\rangle = 1/\sqrt{2}(|0,1\rangle + |1,0\rangle) \quad (1)$$

$$|e_2\rangle = 1/\sqrt{2}(|0,1\rangle - |1,0\rangle) \quad (2)$$

The computed normal mode energies are $\varepsilon_1 = 1687$ cm^{-1}, $\varepsilon_2 = 1667$ cm^{-1}. Using Eqn (A5), we find the peptide vibrational energy $\Omega_0 = 1677$ cm^{-1} and coupling $J = 10$ cm^{-1}. We thus obtained the parameters of the one-exciton Hamiltonian represented by the matrix $h_{mn} = \Omega_0\delta_{mn} + J(1-\delta_{mn})$ $(n, m = 1, 2)$. The resulting coupling is consistent with dipole–dipole interaction

$$J = \frac{(\mu_1 \cdot \mu_2) - 3(\hat{\mathbf{m}} \cdot \mu_1)(\hat{\mathbf{m}} \cdot \mu_2)}{|\mathbf{R}_{12}|^3} \quad (3)$$

Using this expression and the computed geometry, we obtain $J = 10$ cm^{-1}, in agreement with the estimate based on the normal modes.

For the sake of third-order spectroscopy, we only need to consider the lowest three levels of each CO vibration. This leads to two different types of doubly excited vibrational states shown in Fig. 2(B). The first are overtones (local) $|2,0\rangle$ and $|0,2\rangle$, where a single bond is doubly excited. The other $|1,1\rangle$ is collective (non-local), where two bonds are simultaneously excited. We shall denote the former OTE (overtone two-excitation) and the latter CTE (collective two-excitation).[32] In general, there are N OTE and $N(N-1)/2$ CTE, for a total of $N(N+1)/2$ states, where N is a number of peptides. The two-exciton manifold consists of linear combinations of the OTE and CTE states. The one- and two-exciton manifolds of glycine dipeptide are calculated in Appendix A.

Copyright © 2000 John Wiley & Sons, Ltd.

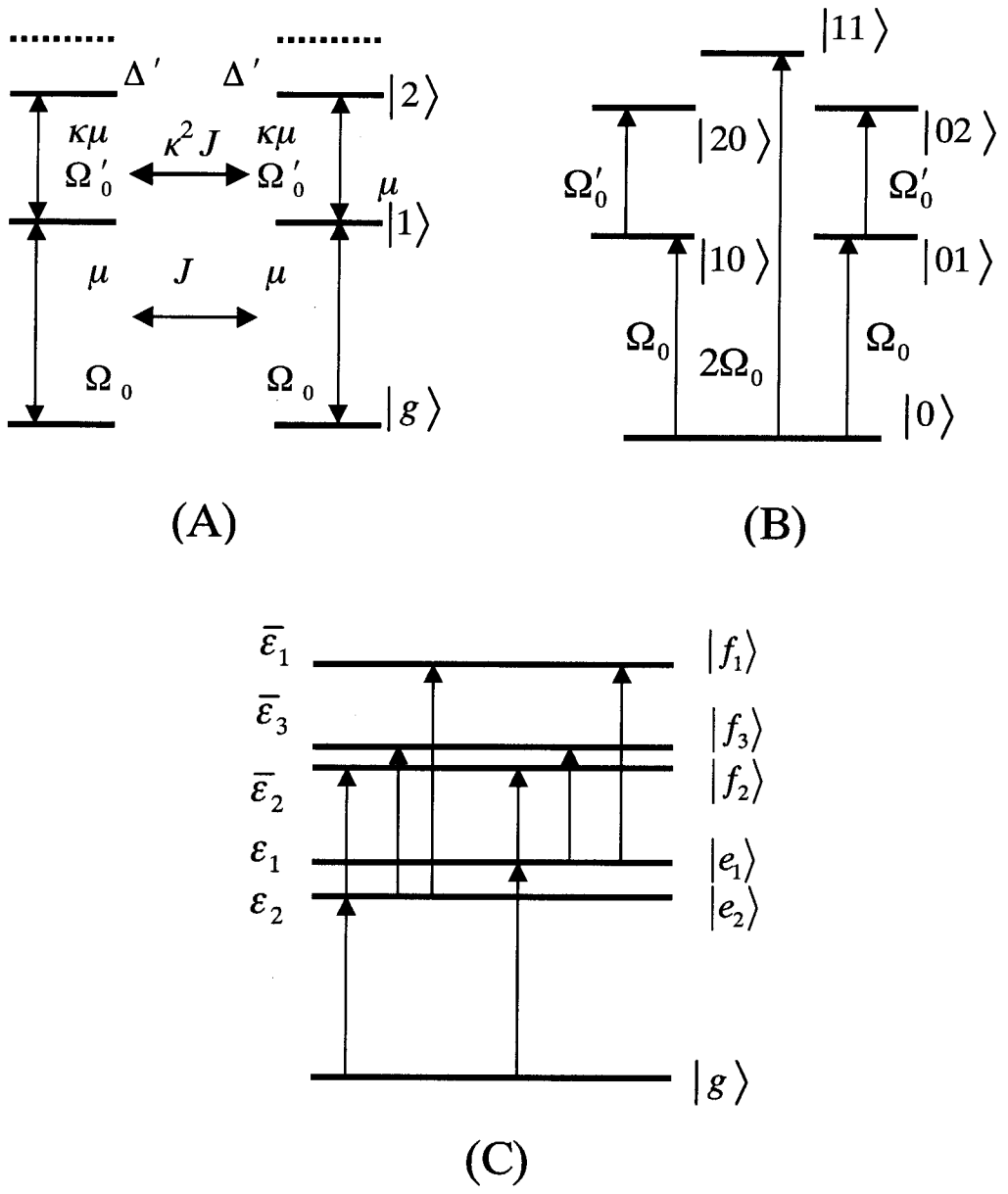

Figure 2. Level diagrams of glycine dipeptide. (A) Peptide units modeled as anharmonic vibrations with 0–1 transition energy Ω_0 and 1–2 transition energy Ω_0', and anharmonicity $\Delta' = \Omega_0' - \Omega_0$. Coupling energy between the vibrations is J and κJ. The 0–1 transition dipole is μ and the 1–2 transition dipole is $\mu' = \kappa\mu$. (B) Excited-state manifold of the two uncoupled ($J = 0$) three-level anharmonic vibrations. States $|1, 0\rangle$ and $|0, 1\rangle$ are single excitation of one of the peptide groups. States $|2, 0\rangle$ and $|0, 2\rangle$ are OTE and state $|1, 1\rangle$ is CTE. (C) Exciton states. Arrows show all possible transitions to one-exciton manifold $\{|e_1\rangle, |e_2\rangle\}$, and between one- and two-exciton $\{|f_1\rangle, |f_2\rangle, |f_3\rangle\}$) manifolds.

The two-exciton manifold is determined by the other two parameters: anharmonicity Δ' and the dipole moment ratio $\kappa = \mu'/\mu$. We took $\Delta' = -16$ cm^{-1} from experiment[22,23] and $\kappa = \sqrt{2}$ corresponds to a harmonic mode. The coupling $\kappa^2 J$ [Eqn (A6)] between the OTE and CTE leads to the formation of the two-exciton states $\{|f_\beta\rangle\}$, $\beta = 1, 2, 3$ [Fig. 2(C)]. Using Eqns (A7) and (A10) and the above parameters we obtain

$$|f_1\rangle = 0.40(|2, 0\rangle + |0, 2\rangle) + 0.83|1, 1\rangle \quad (4)$$

$$|f_2\rangle = -0.59(|2, 0\rangle + |0, 2\rangle) + 0.56|1, 1\rangle \quad (5)$$

$$|f_3\rangle = 1/\sqrt{2}(|2, 0\rangle - |0, 2\rangle) \quad (6)$$

with energies $\bar{\varepsilon}_1 = 3368$ cm^{-1}, $\bar{\varepsilon}_2 = 3325$ cm^{-1} and $\bar{\varepsilon}_3 = 3338$ cm^{-1} [Eqns (A9) and (A11)].

In summary, we have determined the complete set of parameters characterizing the exciton manifolds [Fig. 2(A)]: transition energy Ω_0, the coupling energy J, the anharmonicity Δ' and the ratio of the transition dipoles κ.

Having established the basic structure and the coupling parameters, we next turn to the line broadening. We have employed the following four models:

(A) Small homogeneous dephasing rates of the first excited state with respect to the ground state $\Gamma = 0.4$ cm^{-1} and doubly excited state with respect to the ground state $\gamma^{(2)} = 0.8$ cm^{-1}. This model uses an unrealistically small linewidth in order to resolve all possible resonances.

(B) Large homogeneous dephasing rate $\Gamma = 25$ cm^{-1} and $\gamma^{(2)} = 50$ cm^{-1}. For these parameters the linear absorption linewidth is comparable to the experiment.[22,23]

Copyright © 2000 John Wiley & Sons, Ltd.

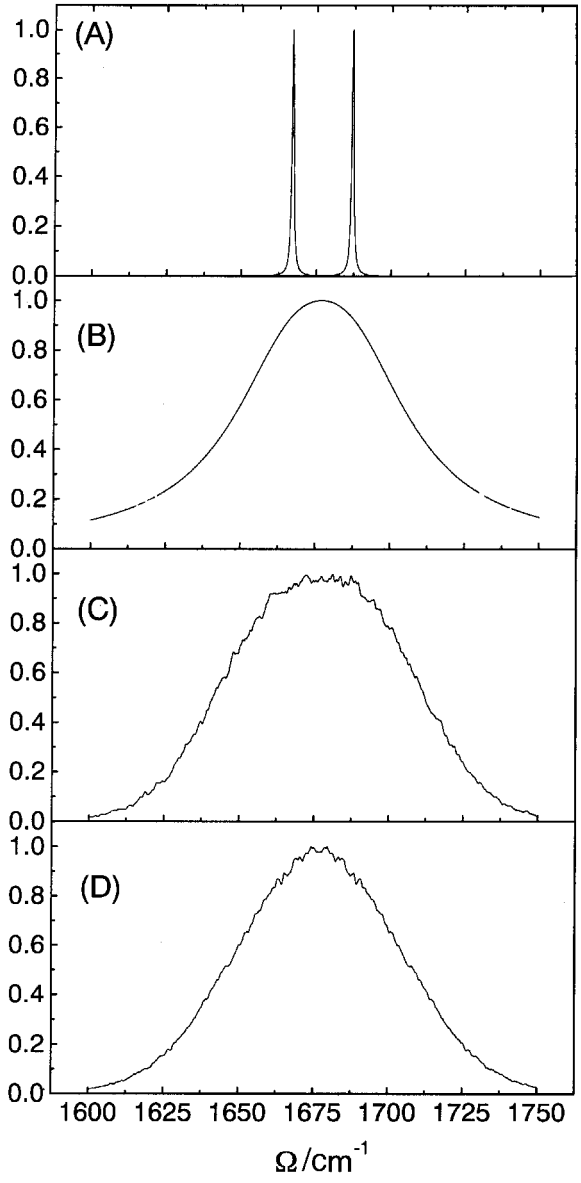

Figure 3. Infrared absorption (1D) spectra of glycine dipeptide for models (A)–(D).

(C) Static diagonal disorder. The nth peptide transition energy is represented as

$$\Omega_n = \overline{\Omega}_0 + \xi_n, \quad n = 1, 2 \tag{7}$$

where $\overline{\Omega}_0$ is the energy average value and ξ_n are random variables representing energy disorder. We assume that both ξ_1 and ξ_2 have uncorrelated Gaussian distributions with the same variance $\sigma_d = 25$ cm^{-1}. The anharmonicity $\Delta' = -16$ cm^{-1} is held fixed, independent on disorder. $\Gamma = 0.4$ cm^{-1} and $\gamma^{(2)} = 0.8$ cm^{-1}.

(D) Static off-diagonal disorder. The coupling is taken to be

$$J = \overline{J} + \zeta \tag{8}$$

where $\overline{J}$ is average coupling energy and ζ is a random variable with a Gaussian distribution with the variance $\sigma_{od} = 25$ cm^{-1}, $\Gamma = 0.4$ cm^{-1} and $\gamma^{(2)} = 0.8$ cm^{-1}. Anharmonicity $\Delta' = -16$ cm^{-1} is held fixed, independent of disorder. In models (C) and (D) the disorder variances σ_d and σ_{od} are chosen to coincide with the homogeneous decay rate in model (B) in order to reproduce total broadening compatible with experiment.[22,23]

The infrared absorption spectra for these models are displayed in Fig. 3. In the absence of disorder the one-exciton states are delocalized. Disorder may lead to exciton localization. In order to describe the degree of exciton localization we have computed the inverse participation ratio[33–35]

$$P(\varepsilon) = \left\langle \sum_{n=1}^{2} |\psi_\varepsilon(n)|^4 \right\rangle^{-1} \tag{9}$$

where $\psi_\varepsilon(n)$ is the nth component of one-exciton wavefunction with energy in the interval $[\varepsilon, \varepsilon + d\varepsilon]$. For a dimer it varies between $P = 1$ (localized state) and $P = 2$ (delocalized state). The distribution of inverse participation ratios is shown in Fig. 4. For models (A) and (B) the exciton states are completely delocalized and their participation ratios are the same. In model (C), static disorder induces exciton localization, and the participation ratio has the value ~1.4 at the maximum. The localized one-exciton manifold coincides with the first excited vibrational state of a single peptide and the two-exciton manifold reduces to the overtone vibrational state. In contrast to diagonal disorder, off-diagonal disorder does not induce exciton

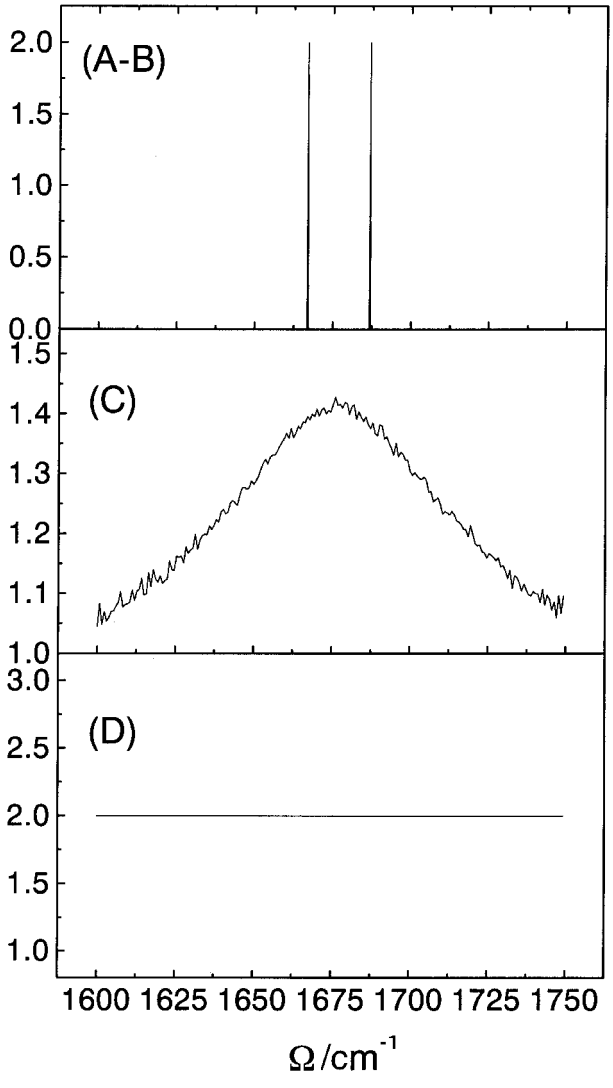

Figure 4. Inverse participation ratio of single exciton states for models (A)–(D).

Copyright © 2000 John Wiley & Sons, Ltd.

localization. This is clearly seen from the inverse participation ratio shown for model (D) {the one-exciton wavefunctions [Eqn (A1)] of model (D) and, consequently, the inverse participation ratio are independent of disorder}.

2D PHOTON ECHOES FOR VARIOUS LINE BROADENING MECHANISMS

The expression for the 2D PE heterodyne signal $S_I(\Omega_2, \Omega_1) = S_I^{(1)}(\Omega_2, \Omega_1) + S_I^{(2)}(\Omega_2, \Omega_1)$ was derived previously.[25] The first component $S_I^{(1)}(\Omega_2, \Omega_1)$ [Eqn (E1) in Ref. 25] represents correlations between one-exciton states shown by the Feynman diagram [Fig. 5(1)].* The second component $S_I^{(2)}(\Omega_2, \Omega_1)$ [Eqn (E2) in Ref. 25] is due to the correlations between one- and two-exciton states and is represented by the Feynman diagram in Fig. 5(2). All three incident and the heterodyne pulses have a parallel linear polarization. Numerical work involved the calculation of the exciton-exciton scattering matrix, following the procedure described in Appendix A of Ref. 25, and evaluating the integral in Eqn (E2) in Ref. 25. The 2D PE signal for models (C) and (D) was averaged over 10^5 disorder realizations.

The absolute value $|S_I(\Omega_2, \Omega_1)|$ of the 2D PE signal is shown in Plate 1. In Plate 2 we display separately the two Feynman diagram contributions to the PE signal [$|S_I^{(1)}(\Omega_2, \Omega_1)|$ (left column) and $|S_I^{(2)}(\Omega_2, \Omega_1)|$ (right column)] for our four models. In the following discussion we shall refer also to the 1D spectra of Fig. 3. For model (A), the 1D spectrum [Fig. 3(A)] has maxima at the one-exciton resonances ε_1 and ε_2. The 2D spectra carry additional information. The diagonal 1 $(-\varepsilon_1, \varepsilon_1)$, 1′ $(-\varepsilon_2, \varepsilon_2)$ and the off-diagonal 2 $(-\varepsilon_1, \varepsilon_2)$, 2′ $(-\varepsilon_2, \varepsilon_1)$ peaks are determined by the first component of the signal [Fig. 5(1)], representing various correlations between the one-exciton states. The cross-peaks 3 $(-\varepsilon_1, \overline{\varepsilon}_1 - \varepsilon_1)$, 4 $(-\varepsilon_1, \overline{\varepsilon}_2 - \varepsilon_1)$, 5 $(-\varepsilon_1, \overline{\varepsilon}_3 - \varepsilon_1)$, 3′ $(-\varepsilon_2, \overline{\varepsilon}_1 - \varepsilon_2)$, 4′ $(-\varepsilon_2, \overline{\varepsilon}_2 - \varepsilon_2)$ and 5′ $(-\varepsilon_2, \overline{\varepsilon}_3 - \varepsilon_2)$ represent the correlations between the one-exciton and two-exciton eigenstates [Fig. 5(2)] and provide direct information on the two-exciton energies. An increase in Γ increases the broadening of the cross peaks in all directions and for model (B), with $\Gamma > (\Delta', J)$, both 1D and 2D spectra are unresolved.

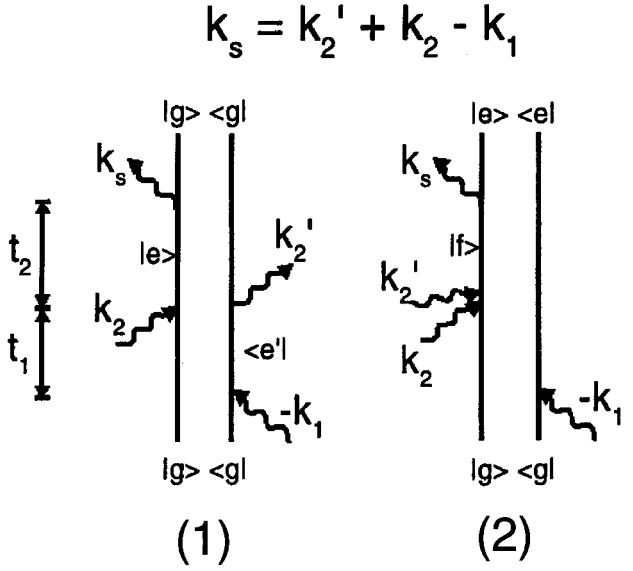

Figure 5. Double-sided Feynman diagrams, representing the two Liouville space pathways contributing to photon echo representing (1) correlations between one-exciton states and (2) correlations between one- and two-exciton states.

* The components of the signal calculated according to these diagrams, using the sum-over-states approach, coincide with those obtained in Ref. 25 in the narrow line limit $\Gamma \ll (\Delta', J)$.

The 1D IR absorption spectra of models (B)–(D) are similar. In contrast, the 2D spectra are very different, illustrating the capacity of 2D spectra to distinguish between the various broadening mechanisms. The 2D spectra of model (C) show inhomogeneous broadening of all peaks of model (A), along the $-\Omega_1 = \Omega_2$ direction. On the other hand, as a consequence of exciton localization on a single chromophore for most realizations of disorder, the 2D spectra show two resonances. One of them is represented by the inhomogeneously broadened diagonal peak 1″ $(-\Omega_0, \Omega_0)$, due to the self-correlation of $|1, 0\rangle$ and $|0, 1\rangle$ states of a single peptide unit. The other is the inhomogeneously broadened cross peak 2″ $(-\Omega_0, -\Omega_0 - \Delta')$ due to the correlation of the single excited states $|1, 0\rangle$ and $|0, 1\rangle$ with the $|2, 0\rangle$ and $|0, 2\rangle$ OTE states. The inhomogeneously broadened 2D resonances associated with the localized exciton states represent the signals stretched along the $-\Omega_1 = \Omega_2$ direction, and marked in Plate 1(C) by dotted lines 1″ and 2″, respectively. For comparison, in the inset in Plate 1(C) we show the inhomogeneously broadened signal of the glycine dipeptide calculated by setting $J = 0$ in model (C). This signal consists of the two resonances alone. An additional, weaker, unmarked feature in Plate 1(C) originates from the inhomogeneous broadening of the cross peaks 3–5 and 3′–5′ shown in Plate 1(A). The anharmonicity Δ' can be obtained from Plate 1(C), as the Ω_2 distance between maxima 1″ and 2″, for fixed Ω_1. The homogeneous relaxation parameters can also be obtained from the same plot. The half-widths of the 1″ and 2″ signals along Ω_2 for a fixed value of Ω_1 give Γ and $\gamma^{(2)} + \Gamma$, respectively.

The 2D signal in model (D) reflects some very special properties of a symmetric dimer with off-diagonal disorder: the one-exciton wavefunctions, the two-exciton wavefunction of the state $|f_3\rangle$ and the energies $\varepsilon_1 + \varepsilon_2$ and $\overline{\varepsilon}_3$ do not depend on a disorder realization. This implies that, in contrast to model (C), some of the cross peaks are broadened in directions different from $-\Omega_1 = \Omega_2$. The 2D spectrum in Plate 1(D) is dominated by the inhomogeneously broadened in the $-\Omega_1 = \Omega_2$ direction diagonal peaks $(-\varepsilon_1, \varepsilon_1)$, $(-\varepsilon_2, \varepsilon_2)$, marked by the dotted lines 1 and 1′, and the inhomogeneously broadened in the same direction cross peaks $(-\varepsilon_1, \overline{\varepsilon}_1 - \varepsilon_1)$ and $(-\varepsilon_2, \overline{\varepsilon}_2 - \varepsilon_2)$ related to the two-exciton mixed states, and marked by the dotted lines 3, and 4′, respectively. We also note that the inhomogeneously broadened peaks 1 and 3 are stretched only in the upper half-plane whereas peaks 1′ and 4′ stretch in the lower half-plane. There is no contribution to the spectrum from the off-diagonal peaks $(-\varepsilon_1, \varepsilon_2)$ and $(-\varepsilon_2, \varepsilon_1)$, which if they existed would be represented as an inhomogeneously broadened signal, stretched along the $\Omega_1 = \Omega_2$ direction, since $\varepsilon_1 + \varepsilon_2$ does not depend on a disorder realization. We explain this effect in the next section by looking at the 2D phase behavior. The other weaker broadened cross peaks cannot be clearly resolved,

Copyright © 2000 John Wiley & Sons, Ltd.

producing a background signal. The homogeneous relaxation parameters can be obtained from Plate 1(D) in the same way as described for model (C).

PHASE DISCRIMINATION OF TWO-EXCITON STATES: OVERTONE VS COLLECTIVE TYPE

The 2D signal is complex. Its real and imaginary parts can be probed separately. So far we have considered only its absolute value. Its phase

$$\Phi = \arctan\{Im[S_I(\Omega_2, \Omega_1)]/Re[S_I(\Omega_2, \Omega_1)]\} \qquad (10)$$

carries additional information. The calculation phase of the 2D signals of models (A)–(D) is displayed in Plate 3. For model (A) the phase has a dispersive behavior near the resonances. If the exciton scattering matrix were a real function in the vicinity of each resonance, then the phase discontinuity would take place exactly at the 2D resonance positions. However, it is slightly shifted owing to the additional phase contribution of the complex exciton scattering matrix, which carries information on the two-exciton states [Eqns (4)–(6)]. The phase at each cross peak depends on its relative OTE and CTE character.

The phase of model (A) in the vicinity of off-diagonal peak 2 $(-\varepsilon_1, \varepsilon_2)$ and cross peaks 5 $(-\varepsilon_1, \bar{\varepsilon}_3 - \varepsilon_1)$, 3 $(-\varepsilon_1, \bar{\varepsilon}_1 - \varepsilon_1)$ and 4 $(-\varepsilon_1, \bar{\varepsilon}_2 - \varepsilon_1)$ is displayed in Plate 3(a)–(d) (right column), respectively. Crosses mark the positions of the resonances. It is clearly seen that they are slightly off the discontinuity line (the edge between the red and blue regions). Since spectral lines overlap, the phase of a particular resonance has additional contributions from other resonances. We have subtracted these contributions from each cross- and off-diagonal peaks and summarized the results in Table 1. Expressions for the phase of cross peaks associated with $|f_3\rangle$ and the $|f_1\rangle$ and $|f_2\rangle$ two-exciton state are derived in Appendix D, and given by Eqn (D4) and Eqns (D7)–(D13), respectively. Resonant phase of off-diagonal peaks is also given by Eqn (D1). According to Eqns (D1) and (D4), resonant phase values of off-diagonal peaks 2 $(-\varepsilon_1, \varepsilon_2)$ and 2′ $(-\varepsilon_2, \varepsilon_1)$ and cross-peaks 5 $(-\varepsilon_1, \bar{\varepsilon}_3 - \varepsilon_1)$ and 5′ $(-\varepsilon_2, \bar{\varepsilon}_3 - \varepsilon_2)$ must be identical, as illustrated in Table 1. This suggests that purely OTE resonances can be identified as cross peaks which have the same phase value as off-diagonal peaks. The other (3, 4, 3′ and 4′) cross-peaks related to two-exciton states representing superpositions of OTE and CTE have phase values different from the off-diagonal peaks [Eqn (D8)]. According to Eqn (D8), their values depend only on (Ω_1, Ω_2) coordinates of the cross peaks and their homogeneous widths Γ along the Ω_1 axis for fixed Ω_2 and homogeneous widths $\Gamma^{(2)}$ along the Ω_2 axis for fixed Ω_1. By comparing the cross-peak value measured in an experiment and calculated according to Eqn (D8), the cross peaks associated with superposition of OTE and CTE can be identified.

When model (A) is modified to have $\gamma^{(2)}$ different from 2Γ, the resonant phase has an additional shift given by Eqns (D5) and (D9) induced by the anharmonicity. To illustrate this we set in model (A) $\gamma^{(2)} = 0.4\ \text{cm}^{-1}$. The results are summarized in Table 2. Despite the anharmonicity phase shift, the cross peaks 5 and 5′ associated with OTE still have the same phase as the off-diagonal peaks 2 and 2′. The anharmonicity phase shift $\Delta\phi$ [Eqn (D5)] of the cross peaks 5 and 5′ can be calculated directly from the spectrum, by subtracting ϕ_0 [Eqn (D6)] from the signal phase ϕ. The resonant phase of the cross peaks 3, 3′, 4 and 4′ associated with the two-exciton states representing the mixture of CTE and OTE is different from the phase of the off-diagonal peaks 2 and 2′. The phase shift $\Delta\psi_1$ [Eqn (D9)] of the cross peaks 3 and 3′ and the phase shift $\Delta\psi_2$ [Eqn (D9)] of the cross peaks 4 and 4′ can be determined from the spectrum by subtracting ψ_0 [Eqn (D8)]. It is clearly seen from Table 2 that for different cross peaks associated with the same two-exciton state the anharmonicity phase shift is the same. Increase

Table 1. Phase (in radians) of off-diagonal and cross peaks for the photon echo signal from glycine dipeptide, model (A)[a]

Cross peak	Ω_1 cm^{-1}	Ω_2 cm^{-1}	Γ cm^{-1}	$\Gamma^{(2)}$ cm^{-1}	Phase radi
2	−1687	1667	0.4	0.4	$\chi = \phi_0 = 1.52$
2′	−1667	1687	0.4	0.4	$\chi = \phi_0' = 1.52$
3	−1687	1680.54	0.4	1.2	$\psi_1^{(0)} = 1.45$
3′	−1667	1700.54	0.4	1.2	$\psi_1^{(0)'} = -1.55$
4	−1687	1637.46	0.4	1.2	$\psi_2^{(0)} = 1.56$
4′	−1667	1657.46	0.4	1.2	$\psi_2^{(0)'} = 1.49$
5	−1687	1651	0.4	1.2	$\phi_0 = 1.52$
5′	−1667	1671	0.4	1.2	$\phi_0' = 1.52$

[a] Contributions from other overlapping resonances are subtracted in each case. $\Gamma^{(2)}$ is width of a resonant peak along the Ω_2 axis for fixed Ω_1.

Table 2. Phase (in radians) of off-diagonal and cross peaks for the photon echo signal from glycine dipeptide[a]

Cross peak	Ω_1 cm^{-1}	Ω_2 cm^{-1}	Γ cm^{-1}	$\Gamma^{(2)}$ cm^{-1}	Phase radi
2	−1687	1667	0.4	0.4	$\phi_0 = 1.49, \Delta\chi = 0.03\ \chi = 1.52$
2′	−1667	1687	0.4	0.4	$\phi_0 = 1.49, \Delta\chi = 0.03\ \chi = 1.52$
3	−1687	1680.54	0.4	1.07	$\psi_1^{(0)} = 1.47, \Delta\psi_1 = -0.01, \psi_1 = 1.46$
3′	−1667	1700.54	0.4	1.07	$\psi_1^{(0)'} = -1.55, \Delta\psi_1 = -0.01, \psi_1' = -1.56$
4	−1687	1637.46	0.4	0.93	$\psi_2^{(0)} = 1.56, \Delta\psi_2 = -0.03, \psi_2 = 1.53$
4′	−1667	1657.46	0.4	0.93	$\psi_2^{(0)'} = 1.52, \Delta\psi_2 = -0.03, \psi_2' = 1.49$
5	−1687	1651	0.4	0.8	$\phi_0 = 1.55, \Delta\phi = -0.03, \phi = 1.52$
5′	−1667	1671	0.4	0.8	$\phi_0 = 1.55, \Delta\phi = -0.03, \phi = 1.52$

[a] Model (A) is modified by setting $\gamma^{(2)} = 0.4\ \text{cm}^{-1}$. Contributions from other overlapping resonances are subtracted in each case. $\Gamma^{(2)}$ is width of a resonant peak along the Ω_2 axis for fixed Ω_1.

Copyright © 2000 John Wiley & Sons, Ltd.

in inhomogeneous broadening corresponds to strong line overlap and as shown for model (B) none of the peaks in model (A) may be resolved.

Interference effects due to the phase are important for 2D signals in models (C) and (D). By looking at panels (A) and (a)–(d) in Plate 3 we note that in the vicinity of each resonance the phase varies slowly and can be approximated as a constant along the $-\Omega_1 = \Omega_2$ direction. In contrast, it shows fast dispersive behavior along the $\Omega_1 = \Omega_2$ direction. This behavior is the same for the resonances due to the localized exciton states in model (C) for each disorder realization. For close disorder realizations, the resonances stretched along the $-\Omega_1 = \Omega_2$ direction are in-phase, producing the average signal shown in Plate 3. Here the phase discontinuity (the sharp edge between the blue and the red colors) stretched along the $-\Omega_1 = \Omega_2$ direction occurs near the $3''$ resonance. The phase jump (the edge between the yellow and blue regions) stretched parallel to $3''$ is resonance $1''$.

The same mechanism corresponds to the formation of the diagonal peaks 1 and $1'$, in addition to cross peaks 3 and $4'$, in model (D). The phase discontinuity lines (the sharp edges between the blue to red regions) and the lines of the phase jump (the sharp edges between the yellow to blue regions) reproduce the directions of inhomogeneous broadening. However, for close disorder realizations, the signal represented by the off-diagonal peaks, stretched along the $\Omega_1 = \Omega_2$ direction, is out of phase and vanishes. This is the case since the phase of each off-diagonal peak has fast dispersive behaviour in the $\Omega_1 = \Omega_2$ direction. The background signal seen in Plates 1 and 2 is due to the contribution of the other cross peaks, which are stretched in directions different from $-\Omega_1 = \Omega_2$. Their weak intensities can be explained in the same way as for the off-diagonal peaks.

DISCUSSION

In this work we have applied non-linear exciton equations (NEE) to calculate the 2D PE signal from glycine dipeptide in the amide I spectral region. Glycine dipeptide is the simplest molecule whose vibrational CO motion can be described as delocalized exciton states. It is also the simplest model which allows for OTE and STE states. The signal has been calculated for different models of line broadening, which reproduce the total IR (1D) absorption spectra. In contrast to 1D spectra, completely different 2D patterns were obtained for various models of the homogeneous and inhomogeneous broadening (diagonal or off-diagonal static disorder). By performing the 2D PE heterodyne experiment, one can measure the real and imaginary parts of the signal separately, and obtain its absolute value as well as the phase. In particular, we have demonstrated how phase measurement is sensitive to the relative OTE and STE character of the state as well as how 2D inhomogeneous signal depends on the phase variations in different directions.

Both diagonal disorder due to the interaction of peptide groups with local environment and off-diagonal disorder due to the slow conformational fluctuations exist in proteins. The diagonal disorder variance was obtained by fitting of 2D pump–probe spectra in Ref. 22; however, off-diagonal disorder was taken into account by averaging the signal over different conformations of proteins available from NMR and x-ray studies and no value of its variance has been determined. It should be possible to determine this value once the effect of the off-diagonal disorder on 2D spectra is known. This may require the employment of different models for the coupling energy distribution. Complete delocalization of exciton states in the presence of off-diagonal disorder for glycine dipeptide holds only for dimers. For larger peptides the localization within pairs of peptide groups and other disorder-induced effects can take place.[36,37] Slow conformational motion of proteins[38,39] can also be detected by observing the changes in inhomogeneously broadened spectra and distinguishing the off-diagonal contribution.

We have demonstrated that one- and two-exciton homogeneous dephasing rates can be obtained from PE signal as the Ω_2 half-widths of the diagonal and off-diagonal peaks. The two-exciton homogeneous dephasing rate is the Ω_2 half-widths of the cross peaks. Dynamic hole burning experiments[22,23] were employed to measure the one-exciton state relaxation parameters and its values have been well established. However, the two-exciton state dephasing rate in amide I region, which may reveal new information related to the CO group coupling with intra-protein vibrational modes, has not been reported. The value of the 1–2 dephasing rate was measured using the PE technique for a single CO group attached to the hemo pocket of hemoglobin protein and several model molecules.[21]

Two-dimensional PE measurement can also provide the value of the vibrational anharmonicity. In polypeptides with well localized excited states, knowledge of each is important for structure determination.[23] Since 2D PE spectroscopy is a femtosecond impulsive technique, it can be used for real-time study of early events in protein folding, which are the focus of extensive effort. Two-dimensional NMR spectroscopic methods[27] are limited to much slower time-scales (milliseconds), hence 1D IR[3–7] and luminescence[40] spectroscopy are employed for following faster conformational changes. Two-dimensional IR spectroscopy should provide more detailed information.

The advantage of the NEE approach is that modeling of the two-exciton dynamics requires calculation of the exciton scattering matrix which scales as N^2, where N is number of peptide units. The total 2D signal computational time scales as $\sim N^4$, allowing further application to study the response of small polypeptides and average the signal over a sufficient number of Monte Carlo runs to account for the static disorder. Moreover, interference effects are naturally built-in, making it particularly suitable for inverting 2D signals to yield the structure and dynamic parameters. The pump–probe simulations of Refs 22 and 23 were carried out using the sum over one- and two-exciton states approach. This requires the diagonalization of the two-exciton Hamiltonian, which scales as N^4. The total 2D signal computational time scales as $\sim N^6$ in this case. The NEE which take into account the coupling with a thermal bath allows one also to model the exciton relaxation dynamics. In particular, the calculation based on the exciton scattering matrix accounts for the renormalization of the two-exciton dephasing rate

Copyright © 2000 John Wiley & Sons, Ltd.

[provided $2\Gamma \neq \gamma^{(2)}$], determined by the relative contribution of OTE and CTE to a specific two-exciton state.

Finally, we note that the other 2D techniques proposed in Ref. 25 can be complementary to PE spectroscopy and can also be modeled using NEE. In particular, energy equilibration in proteins and polypeptides[22,23] can be observed using the transient grating and the reverse transient grating techniques.

Acknowledgments

The support of the National Science Foundation and the United States Air Force Office of Scientific Research is gratefully acknowledged.

REFERENCES

1. Krimm S, Bandeker J. *Adv. Protein Chem.* 1986; **38**: 181.
2. Surewicz WK, Mantsch HH. *Biochim. Biophys. Acta* 1988; **952**: 115; Surewicz WK, Mantch HH, Chapman D. *Biochemistry* 1993; **32**: 389; Jeckson M, Mantsch H. *Crit. Rev. Biochem. Mol. Biol.* 1995; **30**: 95.
3. Phillips CM, Mizutani Y, Hochstrasser RM. *Proc. Natl. Acad. Sci. USA* 1995; **92**: 7292.
4. Williams S, Causgrove TP, Gilmanish R, Fang KS, Callender RH, Woodruff WH, Dyer RB. *Biochemistry* 1996; **35**: 691.
5. Reinstadler D, Fabian H, Backmann J, Naumannl D. *Biochemistry* 1996; **35**: 15822.
6. Gilmanshin R, Williams S, Callender RH, Woodruff WH, Dyer RB. *Proc. Natl. Acad. Sci. USA* 1997; **94**: 3709.
7. Dyer RB, Gai F, Woodruff WH, Gilmanshin R, Callender RH. *Acc. Chem. Res.* 1998; **31**: 709.
8. Torii H, Tasumi M. *J. Chem. Phys.* 1992; **96**: 3379.
9. Tanimura Y, Mukamel S. *J. Chem. Phys.* 1993; **99**: 9496.
10. Mukamel S, Piryatinski A, Chernyak V. *Acc. Chem. Res.* 1999; **32**: 145.
11. Mukamel S. *Principles of Nonlinear Optical Spectroscopy.* Oxford University Press: New York, 1995.
12. Piryatinski A, Chernyak V, Mukamel S. In *Ultrafast Phenomena XI*, Elsaesser T, Fujimoto JG, Wiersma DA, Zinth W (eds). Springer: Berlin, 1998; 541; Mukamel S, Piryatinski A, Chernyak V. *J. Chem. Phys.* 1999; **110**: 1711.
13. Zhang WM, Chernyak V, Mukamel S. In *Ultrafast Phenomena XI*, Elsaesser T, Fujimoto JG, Wiersma DA, Zinth W (eds). Springer: Berlin, 1998; 663; Mukamel S, Zhang WM, Chernyak V. In *Photosynthesis: Mechanisms and Effects*, vol. 1, Garab G (ed). Kluwer: Dordrecht, 1998; 3.
14. Okumura K, Tokmakoff A, Tanimura Y. *J. Chem. Phys.* 1999; **111**: 492.
15. Joo T, Jia Y, Yu J-Y, Lang MJ, Fleming GR. *J. Chem. Phys.* 1996; **104**: 6089.
16. Hybl JD, Albrecht AW, Gallagher Faeder SM, Jonas DM. *Chem. Phys. Lett.* 1998; **297**: 307.
17. Loring RF, Mukamel S. *J. Chem. Phys.* 1985; **83**: 2116.
18. Tominaga K, Yoshihara K. *Phys. Rev. Lett.* 1995; **74**: 3061; Tominaga K, Yoshihara K. *Phys. Rev. A* 1997; **55**: 831.
19. Tokmakoff A, Lang MJ, Larsen DS, Fleming GR, Chernyak V, Mukamel S. *Phys. Rev. Lett.* 1997; **79**: 2702.
20. Tokmakoff A, Fleming GR. *J. Chem. Phys.* 1997; **106**: 2569.
21. Rector KD, Kwok AS, Ferrante C, Tokmakoff A, Rella CW, Fayer MD. *J. Chem. Phys.* 1997; **106**: 10027.
22. Hamm P, Lim M, Hochstrasser RM. *J. Phys. Chem. B* 1998; **102**: 6123.
23. Hamm P, Lim M, DeGrado WF, Hochstrasser R. *Proc. Natl. Acad. Sci. USA* 1999; **96**: 2036.
24. Chernyak V, Zhang WM, Mukamel S. *J. Chem. Phys.* 1998; **109**: 9587.
25. Zhang WM, Chernyak V, Mukamel S. *J. Chem. Phys.* 1999; **110**: 5011.
26. Ernst RR, Bodenhausen G, Wokaun A. *Principles of Nuclear Magnetic Resonance in One and Two Dimensions*. Clarendon Press: Oxford, 1987; Sanders JKM, Hunter BH. *Modern NMR Spectroscopy*. Oxford University Press: New York, 1993.
27. van Nuland NAJ, Forge V, Balbach J, Dobson CM. *Acc. Chem. Res.* 1998; **31**: 773.
28. Bach AC, Eyermann CJ, Gross JD, Bower MJ, Harlow RL, Weber PC, DeGrado WF. *J. Am. Chem. Soc.* 1994; **116**: 3207.
29. Frisch Æ, Frisch MJ. *Gaussian 98. User's Reference.* (Gaussian, Inc., (1999)); Foresman JB, Frisch Æ. *Exploring Chemistry with Electronic Structure Methods*. Gaussian: Pittsburgh, PA, 1996.
30. Chem TC, Krimm S. *J. Mol. Struct.* 1989; **193**: 1.
31. Head-Gordon T, Head-Gordon M, Frisch MJ, Brooks CL, III, Pople JP. *J. Am. Chem. Soc.* 1991; **113**: 5989.
32. In Ref. (A1), the OTE are referred as MDE (molecular double excitations) and the CTE as CDE (collective double excitations).
33. Economou E. *Green's Function in Quantum Physics*. Springer: New York, 1994.
34. Thouless D. *Phys. Rep., Phys. Lett.* 1974; **13C**: 93.
35. Spano FC, Kuklinski JR, Mukamel S. *Phys. Rev. Lett.* 1990; **65**: 211.
36. Kozlov GG, Malyshev VA, Dominguez-Adame F, Rodriguez A. *Phys. Rev. B* 1998; **58**: 5367.
37. Meier T, Chernyak V, Mukamel S. *J. Chem. Phys.* 1997; **107**: 8759.
38. Leeson DT, Wiersma DA. *Phys. Rev. Lett.* 1995; **74**: 2138.
39. Leeson DT, Wiersma DA. *Nature Struct. Biol.* 1995; **2**: 848.
40. Ballew RM, Sabelko J, Gruebele M. *Nature Struct. Biol.* 1996; **3**: 923.

APPENDIXES

A: ONE- AND TWO-EXCITON MANIFOLD OF A SYMMETRIC DIMER

In this Appendix, we present expressions for one- and two-exciton eigenstates of a symmetric dimer. Diagonalization of the one-exciton Hamiltonian $h_{nm} = \Omega_n \delta_{nm} + J_{nm}$[24] yields the one-exciton states in the form

$$|e_\alpha\rangle = \sin\theta_\alpha |1,0\rangle + \cos\theta_\alpha |0,1\rangle, \quad \alpha = 1,2 \qquad \text{(A1)}$$

where $|1,0\rangle = B_1^\dagger|0\rangle$, $|0,1\rangle = B_2^\dagger|0\rangle$ and

$$\theta_\alpha \equiv \arctan[(\Omega_2 - \Omega_1)/2J + (-1)^{\alpha+1} \times \sqrt{[(\Omega_2 - \Omega_1)/2J]^2 + 1}] \quad \alpha = 1,2 \qquad \text{(A2)}$$

The one-exciton energies are

$$\varepsilon_\alpha = (\Omega_2 + \Omega_1)/2 + (-1)^{\alpha+1} \times \sqrt{[(\Omega_2 - \Omega_1)/2]^2 + J^2}, \quad \alpha = 1,2 \qquad \text{(A3)}$$

For a symmetric dimer ($\Omega_1 = \Omega_2 \equiv \Omega_0$), one-exciton wavefunctions [Eqn (A1)] simplify to the form

Copyright © 2000 John Wiley & Sons, Ltd.

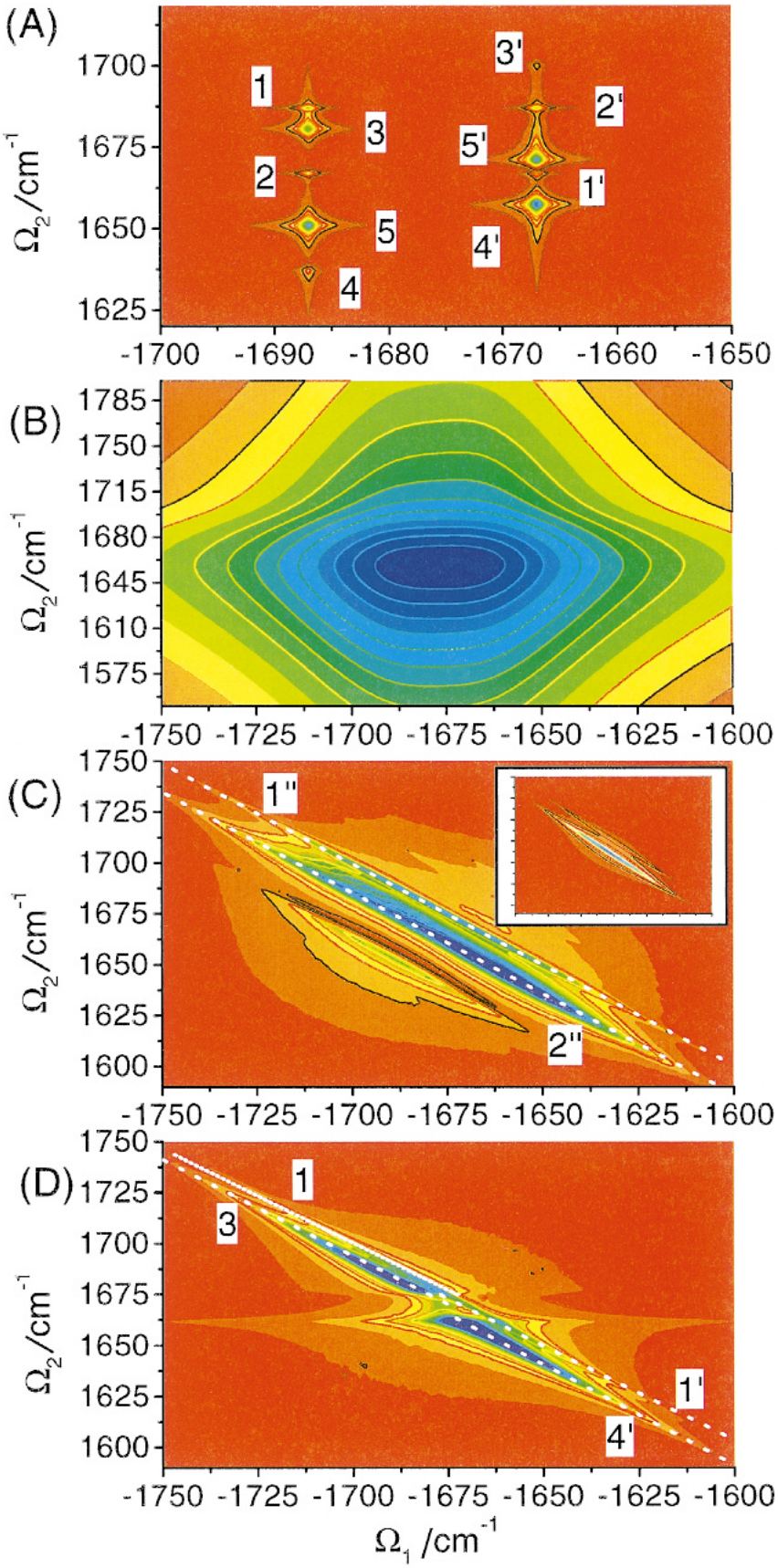

Plate 1. Absolute value $|S_1(\Omega_2,\Omega_1)|$ of 2D infrared photon echo signal from glycine dipeptide for models (A)–(D)

Copyright © 2000 John Wiley & Sons, Ltd.

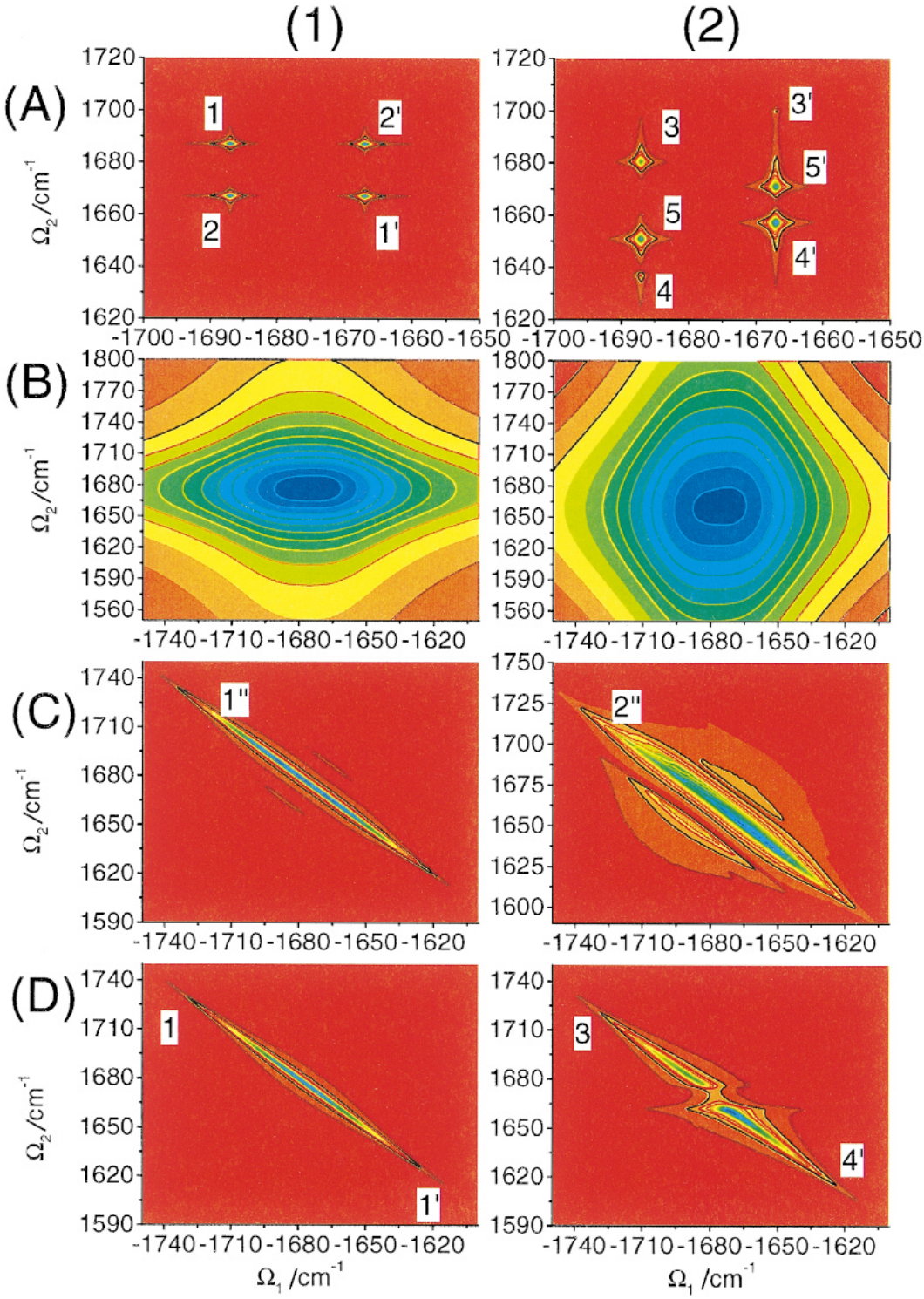

Plate 2. Absolute value of 2D PE signal components (1) $|S_1^{(1)}(\Omega_2,\Omega_1)|$ and (2) $|S_1^{(2)}(\Omega_2,\Omega_1)|$ from glycine dipeptide for models (A)–(D)

Copyright © 2000 John Wiley & Sons, Ltd.

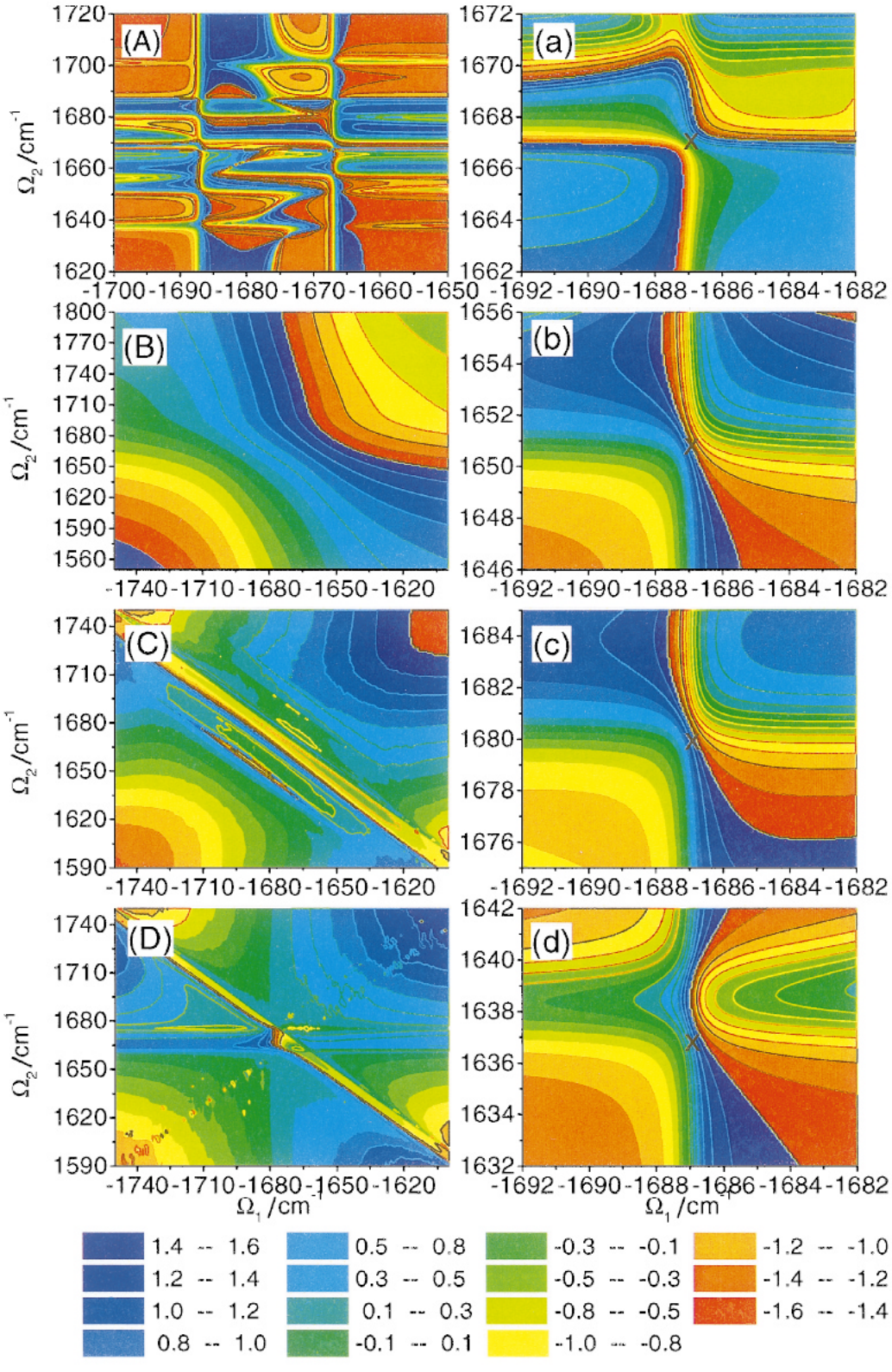

Plate 3. Left column: phase (in radians) of 2D infrared photon echo signal [Eq^{n} (10)] from glycine dipeptide for models (A)-(D). Right column: the phase of panel (A) is displayed on an expanded scale in the vicinity of various resonances: (a) (ε_1, ε_2), (b) (ε_1, $\bar{\varepsilon}_3 - \varepsilon_1$), (c) ($\varepsilon_1$, $\bar{\varepsilon}_1 - \varepsilon_1$) and (d) ($\varepsilon_1$, $\bar{\varepsilon}_2 - \varepsilon_1$)

Copyright © 2000 John Wiley & Sons, Ltd.

$$|e_\alpha\rangle = 1/\sqrt{2}(|1,0\rangle + (-1)^{\alpha+1}|0,1\rangle) \quad \alpha = 1,2 \tag{A4}$$

and the one-exciton energies become

$$\varepsilon_\alpha = \Omega_0 + (-1)^{\alpha+1}J, \quad \alpha = 1,2 \tag{A5}$$

The two-exciton Hamiltonian in the bases set of OTE $|2,0\rangle = (B_1^\dagger)^2|0\rangle$, $|0,2\rangle = (B_2^\dagger)^2|0\rangle$, and CTE $|1,1\rangle = B_1^\dagger B_2^\dagger|0\rangle$ matrix elements of the Hamiltonian given by Eqn (2.4) in Ref. 25, without the radiation and phonon interaction terms, is

$$h^{(2)} = \begin{pmatrix} \kappa^2(\Omega_0 + g/2) & 0 & \kappa^2 J \\ 0 & \kappa^2(\Omega_0 + g/2) & \kappa^2 J \\ \kappa^2 J & \kappa^2 J & 2\Omega_0 \end{pmatrix} \tag{A6}$$

where the ratio κ of the 1–2 transition dipole moment to the 0–1 transition dipole moment determines the exciton statistics. The parameter g is the exciton scattering energy, defined as $g = 2\kappa^{-2}[\Delta' - (\kappa^2 - 2)\Omega_0]$, where $\Delta' = \Omega_0' - \Omega_0$ is the anharmonicity (Ω_0' is the 1–2 transition energy). (In the Hamiltonian of Eqn (A6), $g = Re(\tilde{g})$, where $\tilde{g}$ given by Eqn (B7) is the complex exciton scattering energy appearing in the exciton scattering matrix, when the exciton–phonon interaction is eliminated resulting in the relaxation kernels.) The two-exciton manifold determined by the Hamiltonian [Eqn (A6)] consists of three two-exciton states. Two of them are linear combinations of OTE and CTE:

$$|f_\beta\rangle = \sin\Phi_\beta(|0,2\rangle + |2,0\rangle) + \cos\Phi_\beta|1,1\rangle, \quad \beta = 1,2 \tag{A7}$$

with

$$\Phi_\beta = \arctan\left(\frac{2\Omega_0 - \overline{\varepsilon}_\beta}{2\kappa^2 J}\right), \quad \beta = 1,2 \tag{A8}$$

and the energies

$$\overline{\varepsilon}_\beta = 2\Omega_0 + 1/2[(\kappa^2 - 2)\Omega_0 + \kappa^2 g/2] \times [1 + (-1)^{\beta+1}\sqrt{1 + 2A^2}], \quad \beta = 1,2 \tag{A9}$$

where $A = 2\kappa J/[(\kappa^2 - 2)\Omega_0 + \kappa^2 g/2]$. The other two-exciton state is due to the OTE states only:

$$|f_3\rangle = \frac{1}{\sqrt{2}}(|2,0\rangle - |0,2\rangle) \tag{A10}$$

and has the energy

$$\overline{\varepsilon}_3 = \kappa^2(\varepsilon + g/2) \tag{A11}$$

which does not depend on the coupling J. The structure of the two-exciton states [Eqns (A7) and (A10)] is determined by the dimer symmetry.

B: EXCITON SCATTERING MATRIX FOR A SYMMETRIC DIMER IN THE EXCITON REPRESENTATION

In this Appendix, the expressions for the two-exciton scattering matrix components are derived in the case of a symmetric dimer. The general procedure that we follow to compute $\overline{\Gamma}$ is described elsewhere.[11,24,25,A1,A2] The interaction-free two-exciton Green function of a dimer, in the site representation given by Eqn (B5) in Ref. 25, has the following components:

$$\mathcal{G}_{11}(\omega) = \mathcal{G}_{22}(\omega) = \frac{2[\omega - (\tilde{\varepsilon}_1 + \tilde{\varepsilon}_2)]^2 - [\tilde{\varepsilon}_1 - \tilde{\varepsilon}_2]^2}{2[\omega - 2\tilde{\varepsilon}_1][\omega - 2\tilde{\varepsilon}_2][\omega - (\tilde{\varepsilon}_1 + \tilde{\varepsilon}_2)]} \tag{B1}$$

$$\mathcal{G}_{12}(\omega) = \mathcal{G}_{21}(\omega) = \frac{[\tilde{\varepsilon}_1 - \tilde{\varepsilon}_2]^2}{2[\omega - 2\tilde{\varepsilon}_1][\omega - 2\tilde{\varepsilon}_2][\omega - (\tilde{\varepsilon}_1 + \tilde{\varepsilon}_2)]} \tag{B2}$$

where the complex single exciton energies are denoted $\tilde{\varepsilon}_\alpha = \varepsilon_\alpha - i\Gamma$, $\alpha = 1,2$ and ε_α is given by Eqn (A5). Substitution of Eqns (B1) and (B2) into Eqn (A4) from Ref. 25, inversion of the matrix $F(\omega)$ and its further substitution into Eqn (A3) from Ref. 25 gives the following components of the two-exciton scattering matrix in the site representation:

$$\overline{\Gamma}_{11}(\omega) = \overline{\Gamma}_{22}(\omega) = F_{11}(\omega)[\kappa^2\tilde{g} + \omega(\kappa^2 - 2)]/D(\omega) \tag{B3}$$

$$\overline{\Gamma}_{12}(\omega) = \overline{\Gamma}_{21}(\omega) = -F_{12}(\omega)[\kappa^2\tilde{g} + \omega(\kappa^2 - 2)]/D(\omega) \tag{B4}$$

where

$$F_{11}(\omega) = \kappa^2 - \mathcal{G}_{11}(\omega)[\kappa^2\tilde{g} + \omega(\kappa^2 - 2)] \tag{B5}$$

$$F_{12}(\omega) = -\mathcal{G}_{12}(\omega)[\kappa^2\tilde{g} + \omega(\kappa^2 - 2)] \tag{B6}$$

with the exciton statistics parameter κ, defined in the second section, and the on-site exciton scattering energy:[A1]

$$\tilde{g} = 2\kappa^{-2}[\tilde{\Delta} - (\kappa^2 - 2)\Omega_0] \tag{B7}$$

where $\tilde{\Delta} = \Delta' + i\Delta''$ is the complex anharmonicity. Its imaginary part Δ'' is determined by the irreducible two-exciton operator in the NEE.[24] In this paper we adopt it in the form $\Delta'' = \kappa^2\Gamma - \gamma^{(2)}$. The auxiliary function $D(\omega)$ in Eqns (B3) and (B4) has the following form:

$$D(\omega) = \frac{4[\omega - \tilde{\tilde{\varepsilon}}_1][\omega - \tilde{\tilde{\varepsilon}}_2][\omega - \kappa^2/2(\tilde{\varepsilon}_1 + \tilde{\varepsilon}_2 + \tilde{g})]}{[\omega - 2\tilde{\varepsilon}_1][\omega - 2\tilde{\varepsilon}_2][\omega - (\tilde{\varepsilon}_1 + \tilde{\varepsilon}_2)]} \tag{B8}$$

where

$$\tilde{\tilde{\varepsilon}}_\beta = \tilde{\varepsilon}_1 + \tilde{\varepsilon}_2 + 1/4[\kappa^2\tilde{g} + (\kappa^2 - 2)(\tilde{\varepsilon}_1 + \tilde{\varepsilon}_2)] + (-1)^{\beta+1}\Delta_{12}, \quad \beta = 1,2 \tag{B9}$$

and

$$\Delta_{12} = 1/4\sqrt{[(\tilde{\varepsilon}_1 + \tilde{\varepsilon}_2)(\kappa^2 - 2) + \kappa^2\tilde{g}]^2 + 8\kappa^2(\tilde{\varepsilon}_1 - \tilde{\varepsilon}_2)^2} \tag{B10}$$

In accordance with Eqn (B10) in Ref. 25, the non-vanishing components of the exciton scattering matrix in the exciton basis set are

$$\overline{\Gamma}_{\eta\eta,\alpha\alpha}(\omega) = \frac{[\kappa^2\tilde{g} + (\kappa^2 - 2)\omega][\omega - 2\tilde{\varepsilon}_1][\omega - 2\tilde{\varepsilon}_2]}{4[\omega - \tilde{\tilde{\varepsilon}}_1][\omega - \tilde{\tilde{\varepsilon}}_2]} \tag{B11}$$

$$\overline{\Gamma}_{\eta\alpha,\eta\alpha}(\omega) = \frac{[\kappa^2\tilde{g} + (\kappa^2 - 2)\omega][\omega - (\tilde{\varepsilon}_1 + \tilde{\varepsilon}_2)]}{4[\omega - \kappa^2/2(\tilde{\varepsilon}_1 + \tilde{\varepsilon}_2 + \tilde{g})]} \tag{B12}$$

Copyright © 2000 John Wiley & Sons, Ltd.

where $\eta, \alpha = 1, 2$ and $\eta \neq \alpha$. The real parts of the scattering matrix poles $\tilde{\bar{\varepsilon}}_1, \tilde{\bar{\varepsilon}}_2$ and $\tilde{\bar{\varepsilon}}_3 = \kappa^2/2(\tilde{\varepsilon}_1+\tilde{\varepsilon}_2+\tilde{g})$ represent the two-exciton eigenenergies, while their imaginary parts are related to the two-exciton states dephasing rates. If $\Delta'' = 0$, the real parts of $\tilde{\bar{\varepsilon}}_1, \tilde{\bar{\varepsilon}}_2$ and $\tilde{\bar{\varepsilon}}_3$ coincide with the two-exciton state energies given by Eqns (A9) and (A11). If $\Delta'' \neq 0$, the mixed exciton state energies [Eqn (A9)] are renormalized according to Eqn (B9), while the intrachromophore energy Eqn (A11) stays the same.

C: 2D PE SIGNAL FROM A SYMMETRIC DIMER

In this Appendix, we present the final expressions for 2D PE signal in the wavenumber domain. According to Ref. 25, the photon echo signal has two components. The first component represents the correlations between one-exciton states and is given by Eqn (E1) in Ref. 25. Making substitution of the components of the scattering matrix [Eqns (B11) and (B12)] into Eqn (E1) from Ref. 25, one obtains

$$S_I^{(1)}(\Omega_2\Omega_1) = \frac{i}{4}\sum_{\eta,\nu=1}^{2}\left[\frac{\mu_\eta\mu_\eta\mu_\nu\mu_\nu}{[\Omega_1+\varepsilon_\nu+i\Gamma][\Omega_2-\varepsilon_\nu+i\Gamma]}\right.$$
$$\times\frac{[\kappa^2\tilde{g}+2\varepsilon_\nu(\kappa^2-2)][\varepsilon_\nu-\tilde{\varepsilon}_1][\varepsilon_\nu-\tilde{\varepsilon}_2]}{[2\varepsilon_\nu-\tilde{\bar{\varepsilon}}_1][2\varepsilon_\nu-\tilde{\bar{\varepsilon}}_2][\varepsilon_\nu-\tilde{\varepsilon}_\eta]}$$
$$-(1-\delta_{\eta\nu})\frac{1/2(\mu_\eta\mu_\nu+\mu_\nu\mu_\eta)\mu_\eta\mu_\nu}{[\Omega_1+\varepsilon_\eta+i\Gamma][\Omega_2-\varepsilon_\nu+i\Gamma]}$$
$$\left.\times\frac{\kappa^2\tilde{g}+(\kappa^2-2)(\tilde{\varepsilon}_1+\tilde{\varepsilon}_2)+2(\kappa^2-2)i\Gamma}{\kappa^2/2\tilde{g}+(\kappa^2-2)/2(\tilde{\varepsilon}_1+\tilde{\varepsilon}_2)-2i\Gamma}\right] \tag{C1}$$

In this equation the first term in the brackets corresponds to the diagonal peaks $(-\varepsilon_\nu;\varepsilon_\nu)$, $\nu = 1, 2$, and the second term to the off-diagonal peaks $(-\varepsilon_\nu;\varepsilon_\eta)$, $\eta = 1, 2$, $\nu \neq \eta$.

The second component of the signal given by Eqn (E2) in Ref. 25 represents the correlations between the one- and two-exciton states and directly probes the two-exciton resonances which are determined by the scattering matrix poles. Making substitution of Eqns (B11) and (B12) into Eqn (E2) from Ref. 25 and evaluating the integral over $d\omega$, one obtains

$$S_I^{(2)}(\Omega_2\Omega_1) = -\frac{i}{4}\sum_{\eta,\nu=1}^{2}\left[\sum_{\beta=1}^{2}(-1)^{\beta+1}\right.$$
$$\times\frac{\mu_\eta\mu_\eta\mu_\nu\mu_\nu}{[\Omega_1+\varepsilon_\eta+i\Gamma][\Omega_2-(\tilde{\bar{\varepsilon}}_\beta-\tilde{\varepsilon}_\eta)+2i\Gamma]}$$
$$\times\frac{[\kappa^2\tilde{g}+(\kappa^2-2)\tilde{\bar{\varepsilon}}_\beta][\tilde{\bar{\varepsilon}}_\beta-2\tilde{\varepsilon}_1][\tilde{\bar{\varepsilon}}_\beta-2\tilde{\varepsilon}_2]}{[\tilde{\bar{\varepsilon}}_1-\tilde{\bar{\varepsilon}}_2][\tilde{\bar{\varepsilon}}_\beta-2\tilde{\varepsilon}_\eta-2i\Gamma][\tilde{\bar{\varepsilon}}_\beta-2\tilde{\varepsilon}_\nu]}$$
$$+(1-\delta_{\eta\nu})\frac{\kappa^2}{2}\frac{(\mu_\eta\mu_\nu+\mu_\nu\mu_\eta)\mu_\eta\mu_\nu}{[\Omega_1+\varepsilon_\eta+i\Gamma]}$$
$$\frac{}{[\Omega_2-[\kappa^2/2(\tilde{\varepsilon}_1+\tilde{\varepsilon}_2+\tilde{g})-\tilde{\varepsilon}_\eta]+2i\Gamma]}$$
$$\left.\times\frac{\kappa^2\tilde{g}+(\kappa^2-2)(\tilde{\varepsilon}_1+\tilde{\varepsilon}_2)}{\kappa^2/2\tilde{g}+(\kappa^2-2)/2(\tilde{\varepsilon}_1+\tilde{\varepsilon}_2)-2i\Gamma}\right] \tag{C2}$$

The expression in the brackets is a sum of two terms. The first term has resonances associated with the $|f_1\rangle$ and $|f_2\rangle$ two-exciton states [Eqns (4) and (5)], whereas the other one has resonances associated with the $|f_3\rangle$ two-exciton state [Eqn (6)].

D: RESONANT PHASES FOR A SYMMETRIC DIMER

In this Appendix, the expressions for the resonant values of the 2D PE signal phase are derived starting with Eqns (C1) and (C2). In our derivation we do not account for the contribution of the other resonances into the phase value, originating from the overlap of the spectral lines.

According to Eqn (C1), the resonant phases of the off-diagonal peaks $(-\varepsilon_1, \varepsilon_2)$ and $(-\varepsilon_2, \varepsilon_1)$ are identical and have the form

$$\chi = \phi_0 + \Delta_\chi \tag{D1}$$

where we define

$$\phi_0 \equiv \arctan(\Delta'/[\Delta'' + \kappa^2\Gamma]) \tag{D2}$$

and

$$\Delta_\chi \equiv \arctan(\Delta''/\Delta') \tag{D3}$$

according to Eqn (C2). The resonant phases of the cross peaks $(-\varepsilon_\alpha, \tilde{\bar{\varepsilon}}_3 - \varepsilon_\alpha)$ $(\alpha = 1, 2)$, associated with the $|f_3\rangle$ two-exciton state, are identical and have the form

$$\phi = \phi_0 + \Delta\phi \tag{D4}$$

where ϕ_0 is defined by Eqn (D2) and the phase shift is

$$\Delta\phi \equiv \arctan([\Delta'' - (\kappa^2 - 2)\Gamma]/\Delta') \tag{D5}$$

Equation (D2) can be conveniently recast in terms of the cross-peak coordinates as

$$\phi_0 = \arctan([\Omega_1^{(0)} + \Omega_2^{(0)}]/[\Gamma^{(2)} - \Gamma]) \tag{D6}$$

where $\Omega_2^{(0)} \equiv \tilde{\bar{\varepsilon}}_3 - \varepsilon_\alpha$ is the Ω_2 position of one of the cross peaks and $\Omega_1^{(0)} \equiv -\varepsilon_\beta$ is the Ω_1 position of the other cross peak ($\beta \neq \alpha$, and $\alpha = 1, 2$, $\beta = 1, 2$). $\Gamma^{(2)} = (\kappa^2 - 1)\Gamma - \Delta''$ represents the homogeneous width of the cross peaks along the Ω_2 axis and Γ is its homogeneous width along the Ω_1 axis.

The resonant phase of the cross peaks $(-\varepsilon_\alpha, \tilde{\bar{\varepsilon}}_\beta - \varepsilon_\alpha)$, $\alpha = 1, 2$ and $\beta = 1, 2$ determined by $|f_1\rangle$ and $|f_2\rangle$ two-exciton states [Eqns (4) and (5)], in accordance with Eqn (C2) is

$$\psi_\beta = \psi_\beta^{(0)} + \Delta\psi_\beta \tag{D7}$$

where

$$\psi_\beta^{(0)} \equiv \arctan([\Omega_1^{(\beta)} + \Omega_2^{(\beta)}]/[\Gamma^{(2)} - \Gamma]) \tag{D8}$$

with $\Omega_1^{(\beta)} \equiv -\varepsilon_\alpha$, $\Omega_2^{(\beta)} \equiv \tilde{\bar{\varepsilon}}_\beta - \varepsilon_\alpha$. Equation (D8) means that the phase $\psi_\beta^{(0)}$ is a sum of the (Ω_1, Ω_2) cross-peak coordinates, divided by the difference of its homogeneous widths along the Ω_2 and Ω_1 axis, respectively. The phase shift in Eqn (D7) has three components:

$$\Delta\psi_\beta = \Delta\psi_\beta^{(1)} + \Delta\psi^{(2)} + \Delta\psi_\beta^{(3)}, \quad \beta = 1, 2 \tag{D9}$$

Copyright © 2000 John Wiley & Sons, Ltd.

which are

$$\Delta\psi_{\beta}^{(1)} \equiv \arctan\left[\frac{\Delta''/2 + (\kappa^2-2)/(\kappa^2+2)}{\dfrac{((-1)^{\beta+1}\Delta''_{12} - \Gamma)}{\Delta'/2 + (-1)^{\beta+1}(\kappa^2-2)/(\kappa^2+2)\Delta'_{12}}}\right], \quad \beta = 1, 2 \tag{D10}$$

$$\Delta\psi^{(2)} \equiv \arctan(\Delta''_{12}/\Delta'_{12}), \tag{D11}$$

and

$$\Delta\psi_{\beta}^{(3)} \equiv \arctan(C_{\beta}/[1 + rB_{\beta}]), \quad \beta = 1, 2 \tag{D12}$$

The following auxiliary variables are used in Eqn (D12):

$$C_{\beta} \equiv \frac{[\Delta''/2 + (-1)^{\beta+1}\Delta''_{12} - (\kappa^2-2)\Gamma/2]}{[\Delta'/2 + (-1)^{\beta+1}\Delta'_{12}]} \tag{D13}$$

$$B_{\beta} \equiv [\omega_1 - \omega_2]/[\Delta'/2 + (-1)^{\beta+1}\Delta'_{12}]$$

$$r \equiv [\mu_1\mu_1 - \mu_2\mu_2]/[\mu_1\mu_1 + \mu_2\mu_2]$$

and $\mu_{\alpha}\mu_{\alpha}$ ($\alpha = 1, 2$) are first and second dipoles in Eqn (C2).

REFERENCES

A1. Kuhn O, Chernyak V, Mukamel S. *J. Chem. Phys.* 1996; **105**: 8586.
A2. Chernyak V, Wang N, Mukamel S. *Phys. Rep.* 1995; **263**: 213.

Copyright © 2000 John Wiley & Sons, Ltd.